Needle penetration studies on automotive lithium-ion battery cells: Influence of resistance between can and positive terminal on thermal runaway

Hyojeong Kim [a,*], Abdulbashir Sahebzadeh [a], Hans Jürgen Seifert [b], Carlos Ziebert [b], Jochen Friedl [a]

[a] BMW Group, Battery Cell Competence Center (BCCC), 80935, Munich, Germany
[b] Institute for Applied Materials – Applied Materials Physics (IAM-AWP), Karlsruhe Institute of Technology, Hermann-von-Helmholtz-Platz 1, 76344, Eggenstein-Leopoldshafen, Germany

HIGHLIGHTS

- The principle of floating can is discussed as safety element of automotive LIB cell.
- The safety impact of floating can in a prismatic cell is qualitatively investigated.
- The internal short circuit current is quantitatively measured depending on cans.
- ARC demonstrates the thermal equivalence between floating can and can on potential.
- The experimental methods of nail penetration are optimized and summarized in detail.

ARTICLE INFO

Keywords:
Lithium-ion battery
Safety
Floating can
Internal short circuit
Thermal runaway
Needle penetration

ABSTRACT

Thermal runaway (TR) can be initiated by the heat dissipated from an internal short circuit (ISC). In prismatic cells, a crucial type of ISC is located between the cell can on positive potential and the first anode layer. To enhance the safety, the potential of the can could be adjusted by increasing the ISC resistance, i.e., realizing a floating can, whereas a universal automotive prismatic cell has a can on potential in contrast. This work demonstrates that the floating can mitigates the ISC current and possibly prevents ISC from leading to TR using an advanced needle penetration test. Moreover, the ISC current was quantitatively measured, proving that there is no significant ISC current between floating can and outmost anode, while the ISC with can on potential can cause TR. To demonstrate that such difference originates only from the increased resistance, the equivalence in thermal behaviors between the two types of cans was analyzed by a heat-wait-seek test in an accelerating rate calorimeter. This work provides not only a guidance on designing a safer prismatic cell but also a prospect how the optimized needle penetration test can bring a deeper insight into the internal processes of Lithium-ion cells during mechanical abuse.

1. Introduction

Lithium-ion batteries (LIB) have been widely applied in consumer electronic devices and electric vehicles as energy storage systems because of their high energy density and long cycle-life [1–5]. As the energy density of the single Lithium-ion cell increases due to advances in cell chemistry and cell mechanics, the potential safety issues of cells are becoming more pressing, i.e. thermal runaway (TR) and thermal propagation [4,6]. Especially for the development of battery electric vehicles (BEVs), it is desirable to increase the volumetric energy density of the Lithium-ion cell due to the limitation for a further volumetric expansion of the battery pack, which amounts to currently 220–400 l depending on the size of the BEV [4]. In order to increase driving range and power of BEVs by increasing capacity of the Li-ion battery, cathode active materials with higher reactivity are being applied like NMC with higher Ni ratio [7]. As an example, the capacity of the Li-ion battery

* Corresponding author.
E-mail address: hyojeong.kim@bmw.de (H. Kim).

pack in the BMW i3 has been improved from 60 Ah over 94 Ah to 120 Ah. Along with this general trend of increasing reactivity of the cells, however, a concern in safety has been growing. In 2013, the main battery pack of a Boeing 787 flight from Yamaguchi to Tokyo caught fire. It is assumed that the accident was caused by a cell internal short circuit (ISC) [4,8,9]. Between 2015 and 2018, a total of 15 fire incidents of BEVs (Tesla Model S x 7, BMW I3 x 4, Smart x 2, VW E-Golf x 1, Rimac One x 1) were reported in Europe. In 2019, 113 fire incidents took place only within China. Some incidents occurred while driving (38), while the remaining ones took place in vehicles in stationary states, which were either charging (24) or parking (38) [9]. Compared to other electronic devices such as laptops or phones, a thermal runaway in BEVs is more critical, since battery packs in BEVs consist of a large number of cells connected in series and parallel and an enormous amount of thermal energy can be emitted during TR, if propagation is not prevented within the battery pack [6,10–12].

One of the main causes for a TR is an internal short circuit, which generates so much heat that the local temperature reaches the onset temperature of exothermic reactions within a LIB cell, e.g. SEI decomposition or cathode decomposition [4,13]. Under many different abuse scenarios, ISC appears to trigger ultimately the TR, e.g. mechanical abuse (deformation of separator leads to ISC), electrical abuse (separator pierced by dendrite results in ISC) or thermal abuse (shrinkage or melting of separator causes ISC) [4]. Also metallic defects or contaminations within a cell e.g., a small metal impurity inserted during a production process can cause an ISC when the metallic impurity perforates insulating layers due to swelling forces or by a mechanical defect [3,4,14,15].

Two common battery formats for BEVs, namely, prismatic and cylindrical Li-ion cells employ a metallic can, typically made from aluminum or stainless steel, which surrounds the jelly roll(s) or stack(s) in the cell. For prismatic cells with aluminum can the potential of the can should be higher than >1 V vs. Li/Li^+ so that an alloying reaction between lithium cations from the electrolyte and the aluminum from the cell can is inhibited [16]. To ensure this, the potential of the cell can is typically fixed to the potential of the cathode. For that reason, an ISC is generated, if an electrically conductive particle connects the outermost anode layer in the jelly roll and the aluminum can. As a safety measure to limit the current of this undesirable ISC, a high resistance between the positive terminal and the cell can could be introduced. A cell can connected over an increased electric resistance to the positive terminal is called floating can, while a conventional Li-ion cell can is directly connected to the positive terminal and is called can on potential in the following. The floating can is realized by introducing a highly resistive synthetic between the cell can and the rivet, which connects the positive terminal to the cathode. This is schematically shown in Fig. 1b).

If an ISC is induced by a metal impurity between can and outermost anode, four resistances define the ISC current: the inner resistance of the cell (R_i), the resistance between can and anode (R_{CA}), the resistance of the inserted particle ($R_{particle}$) and the resistance between cell can and cathode (R_{CC}). If a particle between can and anode results in an ISC in a Li-ion cell with can-on-potential, substantial current can flow during ISC with low resistance, $R_{ISC,\ can\ on\ potential}$, since R_{CC} is not present. However, such a high current can be prevented by applying floating can because of the considerably escalated resistance, $R_{CC} > 1$ k Ohm.

$$R_{ISC,\ can\ on\ potential} \approx R_i + R_{CA} + R_{particle}$$

$$R_{ISC,\ floating\ can} \approx R_i + R_{CA} + R_{particle} + R_{CC}$$

In this investigation, ISCs were deliberately triggered using advanced needle penetration tests, to evaluate the resilience of Li-ion cells towards an ISC depending on the type of can. As Huang et al. suggested, there are mainly three challenges in a conventional nail penetration test: 1) a large size of used nail with 3–20 mm, 2) relatively high penetration speed like 8 cm/s or greater and 3) temperature measurement on the surface of the cell, hence no information about the local ISC spot inside a cell can be obtained [13,17]. To overcome those three challenges, the following measures were applied in this work.

1. A thin stainless needle with 1 mm diameter was driven into the cell, limiting the mechanical and thermal impact of the needle on the cell under test; the damage caused by the needle on the cell can was kept to a minimum and the siphoning of thermal energy from the inside of the cell over the needle to ambient air was reduced.
2. The needle penetrated the samples with a slow penetration speed, 0.01–0.03 mm/s. As the thickness of components of automotive cells can be quite small, e.g., the current collector foils are roughly 10 μm in thickness, the needle penetration speed has to be slow in order to understand the effect of individual layers.
3. The ISC current is measured indirectly by replenishing the lost cell capacity due to the ISC with a power supply set to constant voltage mode and connected to the cell. In this manner, it is still not feasible to measure the exact local temperature in the ISC area, but it is possible to quantify the amount of ISC current depending on the type of ISC.

Additional details covering the experimental techniques are given in the following chapter.

This work aims to study mainly the influence of the type of can on thermal runaway features of an automotive LIB prismatic cell using needle penetration test. The only difference in the tested cells lies on the connection of the can to the positive terminal, it is either directly connected (can on potential) or connected via a resistor (floating can). Besides the type of can, all tested cells have the same design in terms of capacity (34Ah), chemistry and cell mechanics, which allows to investigate the influence of the type of the connection between can and the positive terminal.

In the first part of this study, cell voltage and three temperatures on cell surface are investigated during needle penetration tests to qualify the thermal stability of the Lithium-ion cell, depending on the resistance

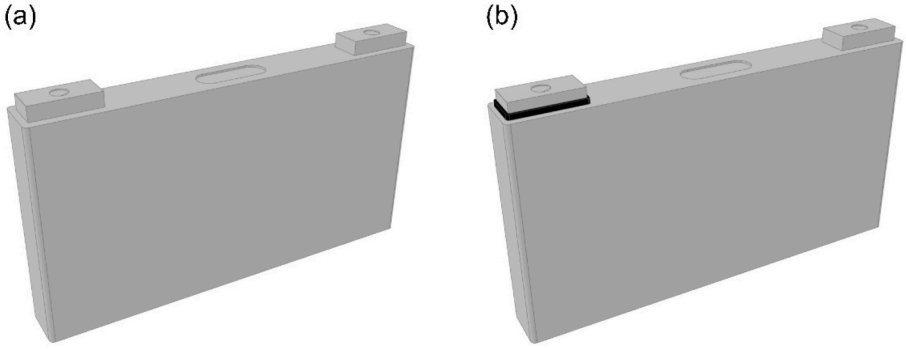

Fig. 1. Li-Ion cell with can on potential (a) and cell with floating can (b).

between cathode and cell can. Every cell was studied under compression, since Lithium-ion cells in EVs are assembled in modules, which are compressed in order to prevent lithium plating due to insufficient contact between the electrodes [18–20]. The obtained results demonstrate that a floating can effectively makes the cells more resilient towards an ISC and prevents a thermal runaway, whereas cells with can on potential experienced severe thermal runaways with hazard levels >4.

In the second part, the method to measure ISC current is studied and the measured ISC current is quantified depending on types of ISC, e.g., ISC between cell can and the outermost anode and ISC between cell layers.

Lastly, the equivalence of the two types of cells in terms of thermal behavior is validated by accelerating rate calorimeter (ARC) tests.

2. Experimental

2.1. Needle penetration test

15 needle penetration tests were carried out to study the impact of the floating can on the safety of LIB cells qualitatively and two additional needle penetration tests were conducted to measure the internal short circuit current quantitatively depending on the type of can.

2.1.1. Linear actuator

All needle penetration tests were conducted using a linear actuator manufactured by Fritz Automation GmbH. A fixed needle can move laterally with speeds from 0.01 to 15 mm/s. Applied forces onto the needle, voltages and temperatures are recorded.

2.1.2. Cell preparation

All tested 17 LIB cells (two jelly rolls, cathode as blend out of NMC111, NMC622 and NCA and anode out of graphite) were fully charged to 100 % state of charge (4.2 V, 34 Ah) by a battery tester at room temperature using a constant current (C/3) - constant voltage (break at I < 1A) protocol. Before charging, every LIB cell was compressed to 5 kN by two stainless-steel plates (210 × 79 × 15 mm^3) with a hole (diameter 15 mm) as shown in Fig. 2a) and b). The applied force is defined in the range of the force that is applied in the real BEV LIB module application and the dimensions of the plates were chosen to compress the entirety of the jelly rolls within the cell.

2.1.3. Test protocol

For every test, needles with a diameter of 1 mm, a length of 60 mm and tip angle of 60° were used. An overview of the performed tests is shown in Table 1. In the first part of tests (1-12), LIB cells were penetrated with controlled speeds (0.01, 0.02 or 0.03 mm/s) until a TR was observed. This was done to compare the critical penetration depth of cells with a floating can and those with can on potential. For each penetration speed, the penetration depth to achieve a thermal runaway was determined twice. Next, three cells with floating can were penetrated at three different speeds, deep enough to achieve an ISC, but not deep enough to trigger a TR (tests 13–15). This was carried out to study the resilience of cells with floating can against ISC. During those needle penetration tests, the following parameters were measured 1) cell voltage, 2) voltage between needle and positive terminal (V_{NP}), 3) voltage between needle and negative terminal (V_{NN}), 4) force applied on needle and 5) temperatures on the surface of cells (on vent, positive and negative terminal) using K-type thermocouple. As the last part, for the quantitative study of the ISC current, the LIB cell was connected via a shunt (40 A, 75 mV) to a power supply (4.2 V, 6 A) as a parallel circuit. In this design, any voltage drops originating from an ISC will be compensated by the power supply to the equivalent voltage of the LIB sample cell in 100 % state of charge, 4.2 V with maximum 6 A. The voltage of the shunt (V_{sh}) was measured additionally, and it was mathematically transformed into current. Since the current flows from power supply over shunt to the cell exactly as much as required to

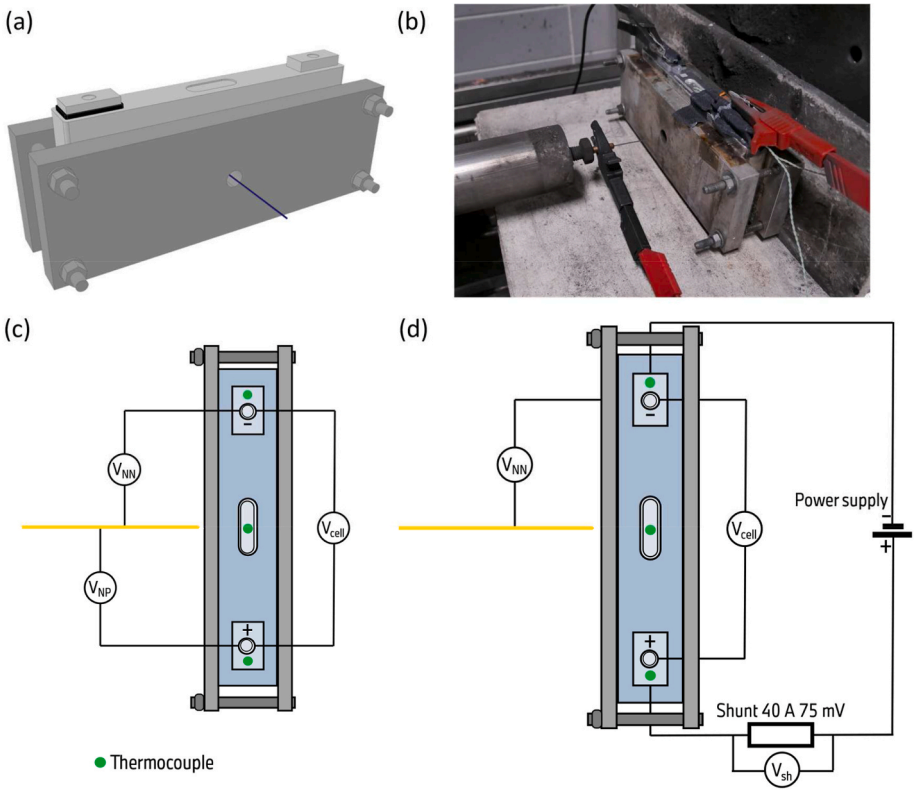

Fig. 2. Test conditions: compressed sample (a), picture of a compressed LIB cell in lab (b), test design for qualitative evaluation of cell type on TR (c) and test design for quantitative measurement of ISC current.

Table 1
Protocol for needle penetration tests.

Test	Type of cell can	Speed of penetration [mm s ^{1}]	Measurement of V				Note
			V_{cell}	V_{NP}	V_{NN}	V_{sh}	
1	Can on potential	0.01	✓	✓	✓	–	penetration until TR (In test 2 and 6, only *d* was determined.)
2		0.01	✓	–	–	–	
3		0.02	✓	✓	✓	–	
4		0.02	✓	✓	✓	–	
5		0.03	✓	✓	✓	–	
6		0.03	✓	–	–	–	
7	Floating can	0.01	✓	✓	✓	–	penetration until TR
8		0.01	✓	✓	✓	–	
9		0.02	✓	✓	✓	–	
10		0.02	✓	✓	✓	–	
11		0.03	✓	✓	✓	–	
12		0.03	✓	✓	✓	–	
13	Floating can	0.01	✓	✓	✓	–	Soft short
14		0.02	✓	✓	✓	–	
15		0.03	✓	✓	✓	–	
16	Can on potential	0.01	✓	–	✓	✓	Measurement of ISC-current
17	Floating can	0.01	✓	–	✓	✓	

replenish the voltage loss from ISC, it can be assumed that this current (I_{sh}) is equivalent to the ISC current. In this supplementary circuit, however, the extent of ISC could be larger than the real ISC where a LIB cell is discharged by ISC, since the lost capacity would be compensated to 100 % state of charge.

From the signal of needle force the penetration depth (*d*) was derived by noting the point of first contact with the cell can and taking the thickness of the cell can (0.69 mm) into account. Furthermore, using two voltage signals between needle and terminals, the penetration depth (*d*) could be optimized as penetration depth from the contact to can (d_{can}) by the exact turning moment to $V_{NN} = 0$ and $V_{NP} = 4.2$ V and as penetration depth from the contact to anode (d_{anode}) by the transition moment to $V_{NN} = 4.2$ and $V_{NP} = 0$ V. All data in the first and second part of tests were recorded by the data acquisition belonging to the linear actuator (100 Hz) and the third part of tests were recorded using Gantner measuring system (100 Hz).

2.2. Accelerating rate calorimeter

2.2.1. Calibration of EV accelerating rate calorimeter

For the ARC tests the extended volume (EV) accelerating rate calorimeter, manufactured by the company Thermal Hazard Technology (THT, Bletchley, Milton Keynes, United Kingdom), was used. Its internal size amounts to 24,540 cm^3 with 25 cm diameter and 50 cm depth and it has one heater and one thermocouple located in the lid and in the bottom; and two heaters and thermocouples (all type N) in the sidewall. The EV ARC allows a tracking of the temperature and temperature rates and operates in (quasi-)adiabatic mode. This means that the cell cannot transfer heat to the calorimeter walls, which represents worst-case conditions. The ARC was calibrated according to the manufacturer recommendations using the calibration mode. A dummy made of aluminum with similar dimensions and heat capacity as the cell and the same thermocouple arrangement were used. In calibration mode, the heater power settings are optimized for uniform heating by determining calibration offsets between the thermocouples. After the calibration, a drift check, which is a standard Heat-Wait-Seek test with the dummy, ensures that the self-heating and self-cooling rate of the dummy stays below 0.02 °C/min.

2.2.2. Cell preparation

Before the ARC test, all four LIB cells (34 Ah) were cycled three times by a battery tester at room temperature using the protocol with a constant current (C/3) - constant voltage (at 4.2 V until I < 1/10C) with a 30-min rest after charging and discharging. After this capacity check, the cell under test was charged to a state-of-charge of 100 % (SOC100) and mounted in the calorimeter chamber. Then, type K and type N thermocouples were attached to the cell with the high temperature resistant adhesive tape. One is in the center of the wide cell surface of the front, which is the main or so-called bomb thermocouple (Type N) that controls the calorimeter temperature. Another thermocouple (Type K) was added on the vent and the cell voltage was monitored as well during the tests.

2.2.3. Heat-wait-seek test

Tests were conducted using the standard heat-wait-seek method from 50 to 350 °C. The HWS test started at 50 °C in the *Heat* Mode by heating up the cell in small temperature steps of 5 °C. At the end of each temperature step the *Wait* Mode was activated for 20 min to establish thermal equilibrium. When the sample chamber and cell were at the same temperature, the system entered the *Seek* mode in which it detected, whether the cell generated heat that leaded to a significant self-heating above the sensitivity limit of 0.02 °C/min. If it was below the limit, the Heat-Wait-Seek loop restarted by heating up the cell by 5 °C. If the limit was exceeded, the system switched to the quasi-adiabatic *Exotherm* mode, i.e. the heaters followed instantaneously the temperature change of the cells' surface. This prevents the heat transfer to the chamber and consequently the cell is heating up more and more until a thermal runaway occurs or the chemicals for this exothermal reaction are completely consumed. When the maximum temperature of 350 °C was reached, the cell was cooled down by introducing compressed air in the *Cooling* mode.

3. Results and discussion

3.1. Influence of the type of can on thermal runaway

Fig. 3 illustrates the voltage and temperature curves of the two groups of LIB cells which were penetrated until TR 1) with can on potential (a, c, e and g), and 2) with floating can (b, d, f and h). Fig. 4 presents the third group of LIB cells with floating can without TR. In all graphs, 0s is the time when the final penetration depth *d* was reached.

In terms of voltage behavior, the reaction of the third group can be defined as soft short, presenting a gradual discharge without a TR, while the first and second group feature a typical behavior of a thermal runaway. Depending on groups, the voltage behaviors can be outlined as below:

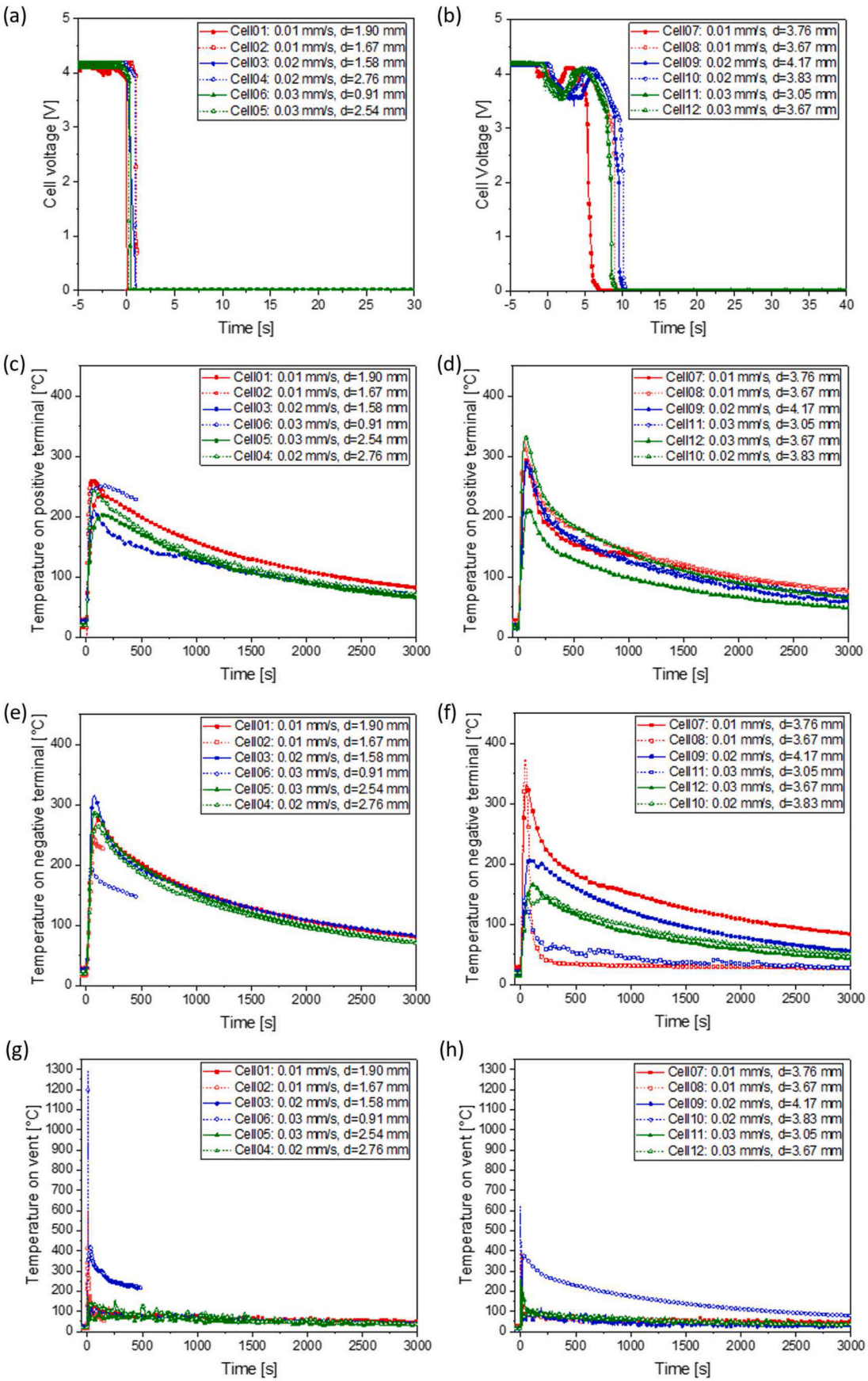

Fig. 3. Cell voltage and temperature profiles of group 1 and 2 with thermal runaway: Cell voltage profile (a), temperature profile on positive terminal (c), on negative terminal (e) and on vent (g) of cell with can on potential; cell voltage profile (b), temperature profile on positive terminal (d), on negative terminal (f) and on vent (h) of cell with can on potential.

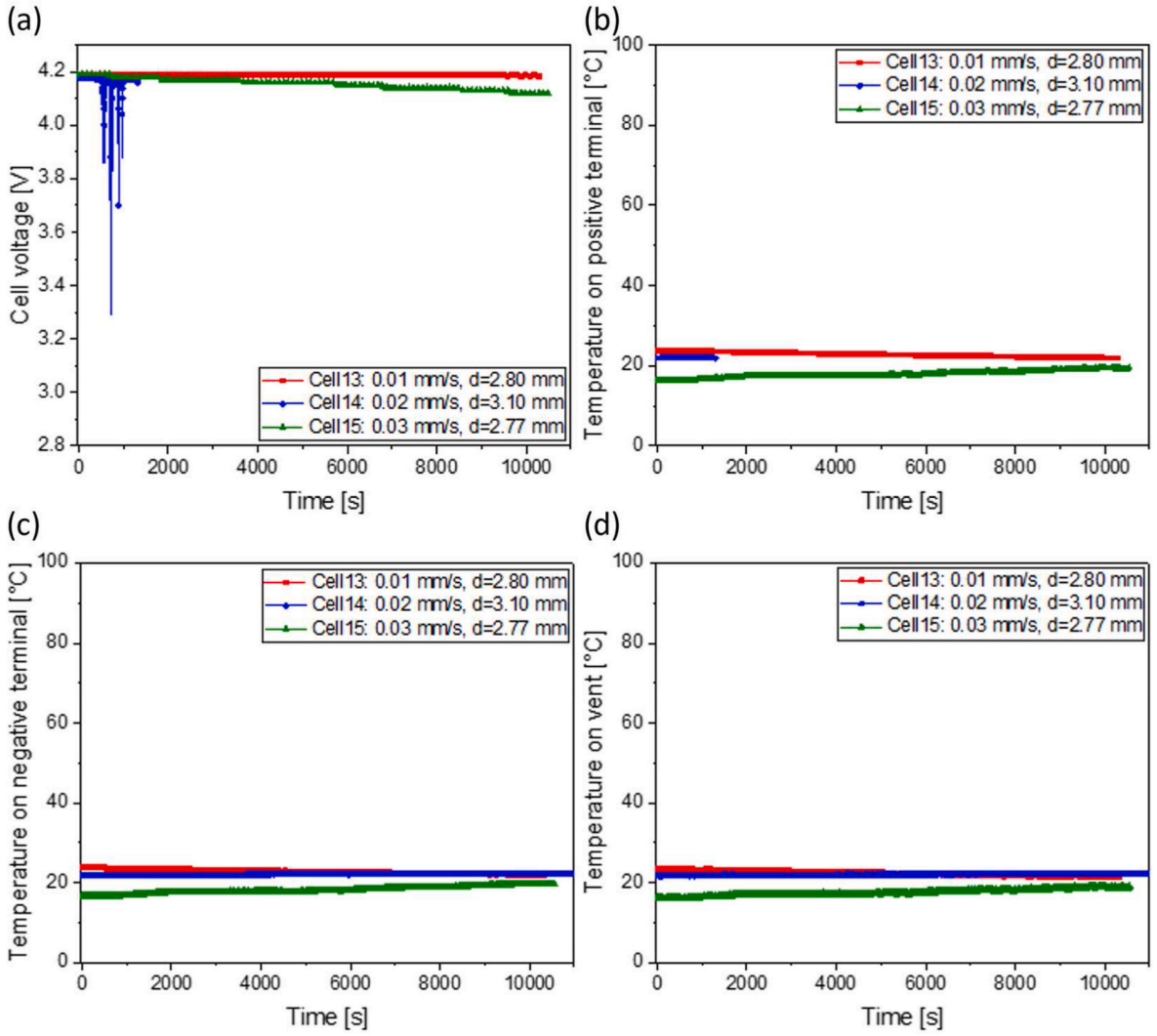

Fig. 4. Cell voltage and temperature profiles of group 3 with soft short: Cell voltage profile (a), temperature profile on positive terminal (b), on negative terminal (c) and on vent (d).

- Group 1: Voltages drop abruptly to 0 V within less than a second after the critical penetration depth was reached (Fig. 3a)).
- Group 2: As soon as the critical *d* was achieved, voltages seem to decline but recover shortly back to 4.2 V then fall to 0 V within a time range of 10 s (Fig. 3b)). This indicates that the short circuit currents are smaller than in the first group and the rise in temperature is slower than in group 1.
- Group 3: Voltages decrease gradually (Fig. 4a)). Especially, the voltage of Cell 14 with the biggest *d* (3.10 mm) in the group presents several fluctuations with the lowest voltage of 3.28 V, showing a resilience against ISC.

To evaluate the behavior of voltages quantitatively, the time to reach 2.8 V, the minimum working voltage of the tested Li-ion cell according to the cell manufacturer, is determined and listed in Table 2.

The evolution of temperatures on positive, negative terminals and vent can be classified also depending on group:

- Group 1: Temperatures on both terminals and vent increase dramatically within 2 s. Maximum values (259 °C on positive terminal, 314 °C on negative terminal and 1289 °C on vent) as seen Fig. 3c), e) and g). Those behaviors correspond to the sudden drop of cell voltage and the jet of flames through the cell vent that was observed. While the temperature on the vent drops abruptly, as soon as the heat is released through an open vent, temperatures on both terminals decrease gradually.
- Group 2: Like Group 1 with can on potential, it shows a typical temperature curve of TR. However, the maximum temperatures on terminals are higher than those of group 1 (Fig. 3d) and f), while the maximum on vent is lower compared to group 1 (Fig. 3h)). It is assumed that the emerged heat from ISC was partially spread broader inside a cell compared to cells with can on potential, because it took longer for voltage to drop with the spring-back phase, while thermal energy in cells of the first group was instantly released mostly through vent.
- Group 3: There are no evident changes in temperatures on the surface of the cells (Fig. 4b), c) and 4d)). Only temperatures of cell 15 increase slightly, since the voltage drop was steeper compared to cell 13 and 14 ($\Delta V = 0.09$ V). Yet, the generated heat was homogenously spread out all inside cells and there is no difference between terminals and vent.

Those experimental results can be supported by the observation of the samples during and after experiments as described below:

- Group 1 and 2: When any cell is penetrated until a critical penetration depth, it experiences a thermal runaway with erupting flame

Table 2
Results of cell 1–15 depending on the type of can and the type of reaction.

Cell in Group 1		01	02	03	04	05	06
Type of can		Can on potential					
Speed of penetration (mm s ^{1})		0.01	0.01	0.02	0.02	0.03	0.03
Penetration depth (mm)	d	1.90	1.67	1.58	2.76	2.54	0.91
	d_{can}	1.90	–	1.80	2.66	2.66	–
	d_{anode}	0.02	–	0.00	0.01	0.01	–
Max. Temp. (°C)	+ Terminal	234.8	259.1	210.1[a]	242	202.5	251.7
	- Terminal	275.0	246.7	314.9	265.2	288.3	251.0
	Vent	600.7	452.8	137.9	173.1	108.1	1288.7
Time to V < 2.8 V		0.02 s	0.97 s	0.00 s	0.91 s	0.20 s	0.40 s
Categorized as		Thermal runaway					
Cell in Group 2		**07**	**08**	**09**	**10**	**11**	**12**
Type of can		Floating can					
Speed of penetration (mm s ^{1})		0.01	0.01	0.02	0.02	0.03	0.03
Penetration depth (mm)	d	3.76	3.67	4.17	3.83	3.05	3.67
	d_{can}	3.76	3.88	4.73	4.05	3.53	3.93
	d_{anode}	1.48	0.88	1.35	1.15	0.77	1.24
Max. Temp. (°C)	Vent	293.8	324.2	289.4	333.7	285.8	212.7
	+ Terminal	331.7	373.5	207.5	149.7[a]	149.4[a]	165.3[a]
	- Terminal	386.1	345.4	116.1	620.8	257.1	123.5
Time to V < 2.8 V		5.35 s	8.79 s	5.08 s	9.02 s	8.05 s	8.07 s
Categorized as		Thermal runaway					
Cell in Group 3		**13**	**14**	**15**			
Type of can		Floating can					
Speed of penetration (mm s ^{1})		0.01	0.02	0.03			
Penetration depth (mm)	d	2.80	3.10	2.77			
	d_{can}	2.81	3.18	3.00			
	d_{anode}	0.20	0.22	0.51			
Max. Temp. (°C)	Vent	No change	No change	19.4			
	+ Terminal			19.6			
	- Terminal			19.1			
Voltage [V] after time [h]		4.16, 24	4.12, 18	4.11, 3			
Categorized as		Soft short					

[a] The considerable difference from the max. temperature on opposite terminal is assumed to result from a defect in thermocouple-adhesive.

and fire (hazard level >5 based on the hazard levels defined by EUCAR).

- Group 3: Cells with floating can experience a slow voltage drop over the course of days without any sudden eruption of flames, even if a nail induces ISC between can and the outmost anode. Additionally, cells that went through soft short remained relatively intact with vent closed (hazard level 3).

In the following Table 2, the summarized results are listed such as penetration depths (d, d_{can} and d_{anode}), the maximum temperatures on positive and negative terminal and vent, time for cell voltage to drop under 2.8 V and type of thermal reactions.

These are the main conclusions drawn by the results given in Table 2:

- The difference between d_{can} and d_{anode} is bigger than the thickness of the studied cell can (0.61 mm). It is assumed that the cell can was pushed by the needle to some extent without penetration of can. Moreover, the penetration depth measured by the applied force on needle, d does not always correspond to the penetration depth (d_{can}) measured by voltage between needle and positive terminal (V_{NP}) or negative terminal (V_{NN}). Those deviations demonstrate why the measurement of voltages, V_{NP} and V_{NN} is necessary to enable the precise detection of the point when the needle has a contact on the can and the outmost anode.
- Cells with can on potential experience a thermal runaway at small $d_{anode} \leq 0.02$ mm with the smallest d_{anode} of 0.00 mm. It is likely that the thermal runaway occurs briefly after or as soon as cell can and outermost anode are shorted by the needle, considering the low resistance against this ISC and the high voltage on this ISC. The applied voltage on this short circuit is quasi-equal to the cell voltage, 4.2 V, since the can is connected to the cathode. The time delay between penetration and voltage drop was less than 1 s indicating that the short circuit between can and outermost anode dissipates a lot of heat quickly, because of the intrinsically low $R_{ISC,\ can\ on\ potential}$, and therefore high short circuit current.
- Cells with a floating can undergo thermal runaway at d_{anode} in the range of 0.77–1.48 mm. As an anode, a cathode and a separator in the tested cell have a thickness of 104 μm, 107 μm and 18 μm, respectively, these penetration depths correspond to 3 to 7 layers. That is because the heat generated by the ISC between can and outermost anode was not enough to trigger the TR and additional shorts between anodes and cathodes were required. In addition, the time until the cell voltage dropped below 2.8 V is slightly longer (5.08–9.02 s) than that of the previously discussed cells with can on potential.
- In the third group, the penetration depth was determined arbitrarily, but sufficiently deep to have a contact between the needle and the electrode ($d_{anode} > 0$). In all three cases, the internal short circuit between cell can and the outmost anode was induced and every LIB cell with floating can experiences a minimal voltage drop without thermal runaway. The discretionally selected penetration depth affects how fast or slows cell voltage drops. For instance, cell 13 with

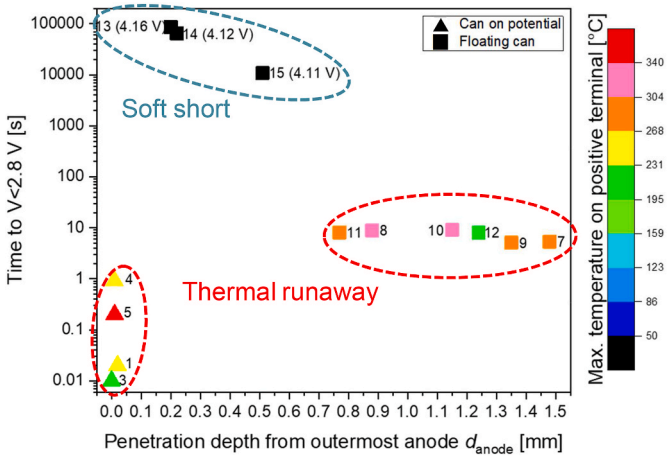

Fig. 5. Classification of Soft short circuit and Thermal runaway depending on can's potential.

the smallest d_{anode} of 0.20 mm demonstrates only 0.04 V drop in 24 h, while it took only 3 h for the voltage of cell 15 with the biggest d_{anode} of 0.51 mm to drop to 4.11 V.

In the following Fig. 5, it can be clearly seen that the cell mechanics, whether the can is on positive potential or connected via a resistance to the positive terminal has a major influence on critical penetration depth, d_{anode}, time to 2.8 V and the type of reaction (TR or soft short). Time to V < 2.8 V is plotted against penetration depth and each sample is colored based on the maximum temperature on the positive terminal. While the smallest measured d_{anode} of cells with floating can is 0 mm, that of cells with can on potential is 0 mm, indicating that thermal runaway occurs by ISC between can and outmost anode in the latter cells.

3.2. Quantitative study of ISC current

Fig. 6 shows the ISC current depending on the type of cell can during the needle penetration. Considering the path of needle penetration inside an automotive prismatic cell, the ISC which takes place first is 1) ISC between cell can and the outmost anode. At second, ISC between cell electrodes and current collectors would arise in the order of 2) ISC between anode and cathode and ISC between anode current collector (Cu) and cathode and 3) ISC between anode and cathode current collector

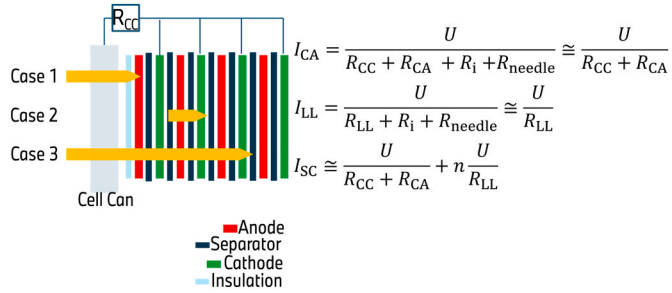

Fig. 7. The short circuit currents in the needle penetration test: the local short circuit between can and outmost anode (case 1), the local short circuit between layers (case 2) and the complex short circuit (case 3).

(Al) and 4) ISC between Cu and Al. Those ISCs that are listed above would come into effect together, as long as the electrical contact between cell layers and needle stays stable without being melted by generated heat or being ruptured (increasing contact resistance).

The cell with can on potential experienced ISC between can and anode as soon as the needle had a contact on the outmost anode (V_{NN}: 4.2 V → 0 V), and the current of ISC increases abruptly until it is limited by the power supply at 6 A (Fig. 6a)), indicating the actual ISC current might have been bigger than 6 A. On the other hand, the cell with floating can does not present any significant ISC current until 16 s (see the first paragraph in section 3.1) even after the needle reached the outmost anode at 88 s. It implies that the current from ISC between can and the outmost anode is negligible because of the high resistance between can and positive terminal. Following the first contact, the current gradually increases while oscillating (Fig. 6b)). It is assumed that the ISC current is constantly increasing as several short circuits are produced and that the observed sharp drops in the current stem from melting or breaking layers in the cell.

Fig. 7 illustrates the short circuit currents that are arising during a needle penetration test with four fundamental resistances, which determine the short circuit current I_{SC} that is induced in dependence of the cell voltage U:

- Case 1: The short circuit current between the cell can and the outermost anode, I_{CA} (see case 1 in Fig. 7) is determined by the resistance between the cell can and the cathode R_{CC}, the resistance between can and the outmost anode R_{CA}, the inner resistance of the

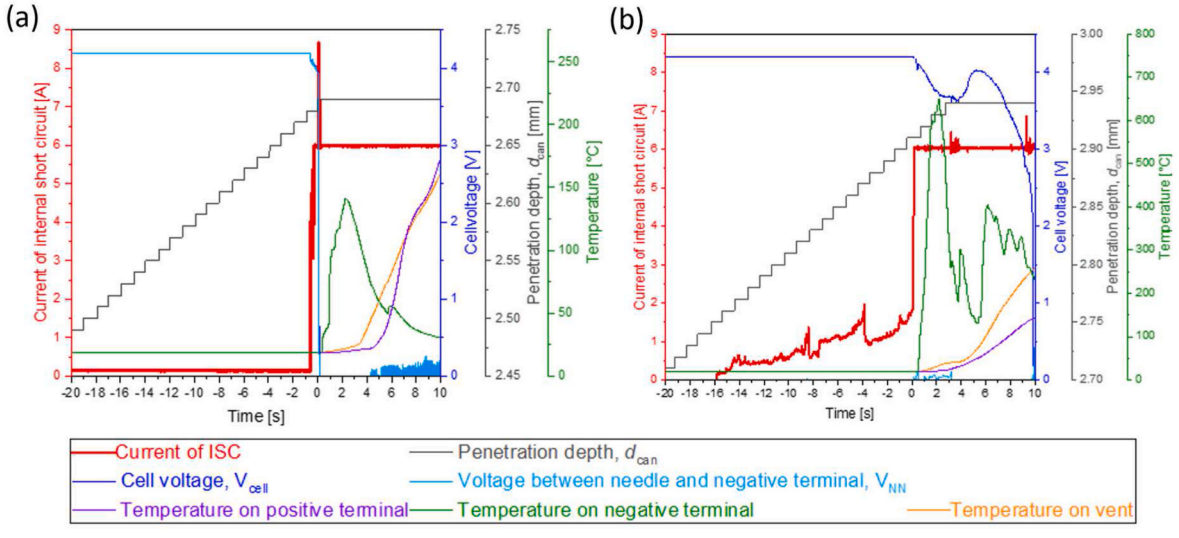

Fig. 6. ISC current measurement: cell with can on potential in the range between −20 and 10 s (a) and cell with floating can in the range between −20 and 10 s (b).

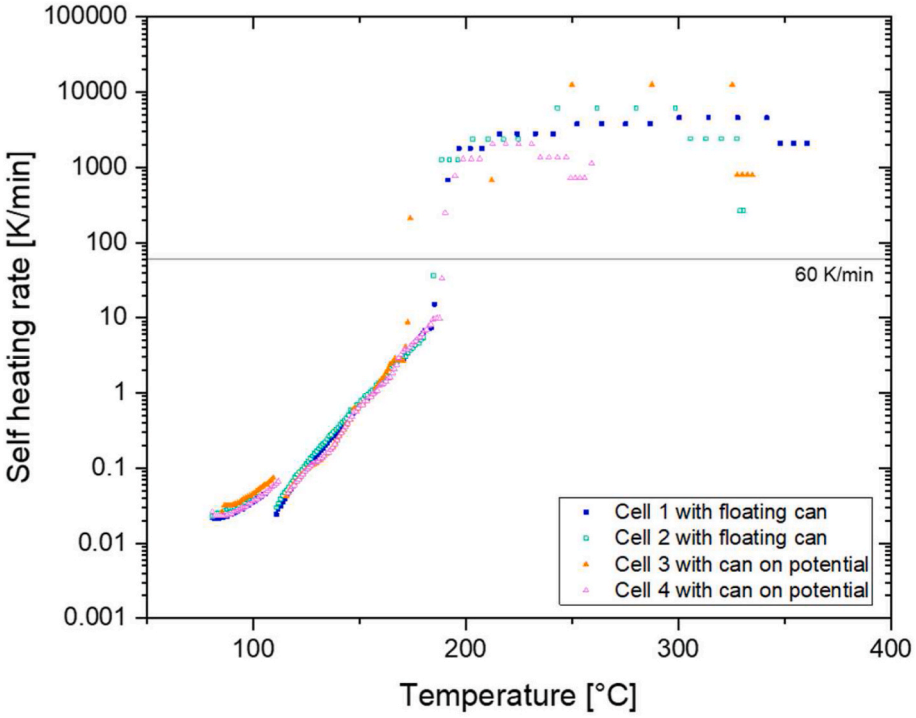

Fig. 8. Self-heating rate of two cells with floating can and two cells with can on potential.

cell R_i and the resistance of the needle R_{needle}. R_{needle} and R_i are negligibly small (<1 mOhm) and can be omitted for this evaluation.

- Case 2: The layer-to-layer short circuit current, I_{LL} (see case 2 in Fig. 7) depends mostly on the layer-to-layer short circuit resistance R_{LL}. For each penetrated pair of anode and cathode n, the short circuit current will increase depending on the number of layer-to-layer short.
- Case 3: Total short circuit current I_{SC} (see case 3 in Fig. 7) is a combination of the short circuit current between the cell can and the outermost anode and the layer-to-layer short circuit current.

In the can on potential configuration R_{CC} is close to zero, hence I_{CA} will be large, which is verified in this work as seen in Fig. 6a) and b). If there is a high resistance R_{CC}, a floating can configuration, however, the I_{SC} via the can is small and the layer-to-layer short circuits contribute the majority of the current. That is why there was no significant current flowing after the contact of needle on the outmost anode until I_{LL} is induced in Fig. 6b). The results shown in Fig. 6 can be interpreted in a way that I_{CA} is much larger than I_{LL} without R_{CC}, thus cells with can on potential experience a thermal runaway from I_{CA} only, no penetration of layers is needed. If the can is floating, however, multiple I_{LL}s are required to discharge the cell.

3.3. Proof of the equivalence in thermal behaviors by heat-wait-seek test in the ARC

Thermal properties of two LIB cells with can on potential and two cells with floating can were compared using ARC to prove that the improved safety of the floating can against internal short circuit between can and outmost anode does not stem from any changes in their thermal properties. Fig. 8 shows the self-heating rate vs. the temperature for all four cells. This curve depicts an average of the data points that were recorded, when the calorimeter was in the *Exotherm* mode. Therefore, the different critical points and regions of the temperature rate can be clearly distinguished, such as the onset point at 80–85 °C, the rate drop due to venting at 103–113 °C, and the point of no return above 168 °C, where the temperature rate exceeded 60 K/min, which means that the cell went into thermal runaway. As seen in Fig. 8 and Table 3, all four cells demonstrate comparable self-heating rates and a good agreement in the five temperature parameters that are given in Table 3. Thus, it can be assumed that the two types of LIB cells have the same thermal properties.

Table 3
Characteristic temperature parameters of two cells with floating can and two cells with can on potential for comparison; T_1 is the onset temperature of the first exothermic reaction due to SEI decomposition (self-heating rate >0.02 K/min), T_2 is the cooling temperature due to venting, T_3 is the onset temperature of the second exothermic reaction (self-heating rate >0.02 K/min), T_4 I the onset temperature ta which the thermal runaway starts (self-heating rate >60 K/min) and T_5 is the maximum temperature during thermal runaway.

Temperature	Floating can		Can on potential	
	Cell 1	Cell 2	Cell 3	Cell 4
T_1 [°C]	80.8	80.8	85.4	80.8
T_2 [°C]	106.6	103.4	108.9	113.2
T_3 [°C]	110.5	112.4	115.2	117.1
T_4 [°C]	168.6	188.6	173.9	190.2
T_5 [°C]	552.1	557.3	326.8	521.7

4. Conclusions

In this work, the impact of the type of LIB prismatic cell can connection on thermal reaction and the ISC current that is depending on it, are studied qualitatively and quantitatively, using a needle penetration test. Furthermore, the equivalence in thermal properties of the two types of cell cans, can on potential and floating can, is proven by ARC. The main conclusions can be drawn as follows.

1. A needle penetration test can reproduce several ISC cases such as an ISC between can and outmost anode and ISC between electrodes and current collectors. In this test, penetration depth is considered as the most important parameter, indicating how robust a LIB cell is against ISC. For the precise diagnosis, voltages between needle and terminals

(V_{NN} and V_{NP}) can be measured so that it is possible to detect the exact contact point of needle to cell can and to the outmost anode, allowing to define the penetration depth from can (d_{can}) and from outmost anode (d_{anode}).
2. The critical penetration depth (d_{anode}) depends on the type of connection between can and positive terminal. An ISC between can and outmost anode can be mitigated by a floating can, demonstrating that the resistance between can and terminal is an effective safety measure. While LIB prismatic cells with can on potential experienced thermal runaway with d_{anode} between 0.00 and 0.02 mm, the critical penetration depth (d_{anode}) of cells with floating can was in the range between 0.77 and 1.48 mm. Moreover, only a gradual self-discharging behavior, representing a soft short was observed, when cells with floating can were penetrated less than 0.51 mm from outmost anode.
3. The current of ISC varies depending on the type of cell:
   i) Can on potential: Because of the intrinsically low R_{CC}, it was observed that ISC_{CA} rose up to the maximum amount (6 A) as soon as the needle bridged can and outmost anode.
   ii) Floating can: No significant ISC_{CA} current was measured due to the high R_{CC}. Thermal runaway seems to originate from the stacking ISC current mostly from ISC_{LL}.
4. According to the result from ARC, the compared two types of LIB cells demonstrate the equivalence of thermal properties. The enhanced safety of floating can does not result from any changes in its thermal behaviors but from its electrical feature.

5. Future work

Further efforts are worthy in the following aspects. First, a measurement of the temperature inside of the cell. As presented in Fig. 3, temperatures on the cell surface change abruptly right after thermal runaway. This makes it challenging to diagnose an inner cell thermal dynamic before thermal runaway. Several researchers have suggested methods to measure the inner temperature by embedding a temperature sensor in a cannula and its benefit [13,21–23]. Second, further systematic investigation of Li-ion cells with different cell chemistry, capacity, assembly and size. These factors could possibly affect the behavior of the cells against ISC and thermal reaction [24]. In the future work, it will be discussed thoroughly which parameter has a major impact on the safety against ISC and what should be profoundly considered in terms of designing a safe automotive LIB cell. Studies of needle penetration could not only contribute to the understanding of the correlation between several crucial factors in cell and safety with respect to ISC but also to fine-tuning the cell chemistry and design.

CRediT authorship contribution statement

Hyojeong Kim: Conceptualization, Methodology, Needle penetration measurement, Accelerating Rate Calorimeter measurement, Analysis, Writing, Editing. **Abdulbashir Sahebzadeh:** Accelerating Rate Calorimeter measurement. **Hans Jürgen Seifert:** Description of ARC measurement, Supervision, review. **Carlos Ziebert:** Description of ARC measurement, Supervision, review. **Jochen Friedl:** Conceptualization, Methodology, Writing – review & editing, Supervision, Project administration.

Declaration of competing interest

The authors declare the following financial interests/personal relationships which may be considered as potential competing interests: Hyojeong Kim reports a relationship with BMW Group that includes: employment. Jochen Friedl reports a relationship with BMW Group that includes: employment.

Data availability

No data was used for the research described in the article.

Acknowledgments

Bayerische Motoren Werke AG is gratefully acknowledged for their financial support. This research was partly funded by the Helmholtz Association, in the programme Materials and Technologies for the Energy Transition (MTET), and we want to express our gratitude for the funding. It contributes to the research performed at CELEST (Center of Electrochemical Energy Storage Ulm-Karlsruhe). We want to thank Nils Uhlmann from the group Batteries - Calorimetry and Safety of the IAM-AWP for instructing and supporting the ARC Measurements.

References

[1] J. Wang, W. Mei, Z. Cui, W. Shen, Q. Duan, Y. Jin, J. Nie, Y. Tian, Q. Wang, J. Sun, Appl. Therm. Eng. 171 (2020), 115082, https://doi.org/10.1016/j.applthermaleng.2020.115082.
[2] T. Yokoshima, D. Mukoyama, F. Maeda, T. Osaka, K. Takazawa, S. Egusa, J. Electrochem. Soc. 166 (2019) A1243–A1250, https://doi.org/10.1149/2.0701906jes.
[3] J. Lamb, C.J. Orendorff, J. Power Sources 247 (2014) 189–196, https://doi.org/10.1016/j.jpowsour.2013.08.066.
[4] X. Feng, M. Ouyang, X. Liu, L. Lu, Y. Xia, X. He, Energy Storage Mater. 10 (2018) 246–267, https://doi.org/10.1016/j.ensm.2017.05.013.
[5] L. Lu, X. Han, J. Li, J. Hua, M. Ouyang, J. Power Sources 226 (2013) 272–288, https://doi.org/10.1016/j.jpowsour.2012.10.060.
[6] J. Duan, X. Tang, H. Dai, Y. Yang, W. Wu, X. Wei, Y. Huang, Electrochem. Energy Rev. 3 (2020) 1–42, https://doi.org/10.1007/s41918-019-00060-4.
[7] S. Cohen, M.K. Gulbinska, F.J. Puglia, in: M.K. Gulbinska (Ed.), Lithium-ion Battery Materials and Engineering, Springer London, London, 2014, pp. 115–150.
[8] N. Goto, All Nippon Airways, Co.Ltd. JA804A, 2014.
[9] Y.-S. Duh, Y. Sun, X. Lin, J. Zheng, M. Wang, Y. Wang, X. Lin, X. Jiang, Z. Zheng, S. Zheng, G. Yu, J. Energy Storage 41 (2021), 102888, https://doi.org/10.1016/j.est.2021.102888.
[10] X. Feng, M. Fang, X. He, M. Ouyang, L. Lu, H. Wang, M. Zhang, J. Power Sources 255 (2014) 294–301, https://doi.org/10.1016/j.jpowsour.2014.01.005.
[11] C.F. Lopez, J.A. Jeevarajan, P.P. Mukherjee, J. Electrochem. Soc. 162 (2015) A1905–A1915, https://doi.org/10.1149/2.0921509jes.
[12] X. Feng, D. Ren, X. He, M. Ouyang, Joule 4 (2020) 743–770, https://doi.org/10.1016/j.joule.2020.02.010.
[13] S. Huang, X. Du, M. Richter, J. Ford, G.M. Cavalheiro, Z. Du, R.T. White, G. Zhang, J. Electrochem. Soc. 167 (2020), 90526, https://doi.org/10.1149/1945-7111/ab8878.
[14] V. Ruiz, A. Pfrang, A. Kriston, N. Omar, P. van den Bossche, L. Boon-Brett, Renew. Sustain. Energy Rev. 81 (2018) 1427–1452, https://doi.org/10.1016/j.rser.2017.05.195.
[15] G. Zhang, X. Wei, X. Tang, J. Zhu, S. Chen, H. Dai, Renew. Sustain. Energy Rev. 141 (2021), 110790, https://doi.org/10.1016/j.rser.2021.110790.
[16] T.R. Jow, C.C. Liang, J. Electrochem. Soc. (1982) 1429–1982.
[17] P. Daniel H. Doughty, Battery Safety Consulting, Inc., Technical Monitor: Ahmad A. Pesaran, Ph.D.: National Renewable Energy Laboratory..
[18] V. Müller, R.-G. Scurtu, K. Richter, T. Waldmann, M. Memm, M.A. Danzer, M. Wohlfahrt-Mehrens, J. Electrochem. Soc. 166 (2019) A3796–A3805, https://doi.org/10.1149/2.1121915jes.
[19] T. Deich, M. Storch, K. Steiner, A. Bund, J. Power Sources 506 (2021), 230163, https://doi.org/10.1016/j.jpowsour.2021.230163.
[20] P. Daubinger, M. Schelter, R. Petersohn, F. Nagler, S. Hartmann, M. Herrmann, G. A. Giffin, Adv. Energy Mater. 12 (2022), 2102448, https://doi.org/10.1002/aenm.202102448.
[21] D.P. Finegan, B. Tjaden, T.M.M. Heenan, R. Jervis, M. Di Michiel, A. Rack, G. Hinds, D.J.L. Brett, P.R. Shearing, J. Electrochem. Soc. 164 (2017) A3285–A3291, https://doi.org/10.1149/2.1501713jes.
[22] T.D. Hatchard, D.D. MacNeil, A. Basu, J.R. Dahn, J. Electrochem. Soc. 148 (2001) A755, https://doi.org/10.1149/1.1377592.
[23] T.D. Hatchard, S. Trussler, J.R. Dahn, J. Power Sources 247 (2014) 821–823, https://doi.org/10.1016/j.jpowsour.2013.09.022.
[24] F. Larsson, J. Anderson, P. Andersson, B.-E. Mellander, J. Electrochem. Soc. 163 (2016) A2854–A2865, https://doi.org/10.1149/2.0131614jes.